Bulletin of the New Zealand Society for Earthquake Engineering, Vol. 57, No. 3, September 2024

PERFORMANCE OF AN ADVANCED SAND CONSTITUTIVE MODEL IN MODELLING SOIL AND SOIL-STRUCTURE INTERACTION UNDER SEISMIC EXCITATION

Piotr Kowalczyk[1]

(Submitted *September 2023*; Reviewed *December 2023*; Accepted *June 2024*)

ABSTRACT

There is a growing number of available advanced soil constitutive models aimed at capturing soil cyclic behaviour and their subsequent use in seismic applications. Nevertheless, detailed validation studies of these soil constitutive models on benchmark experimental works including seismic soil-structure interaction are still rare. This work presents a short validation study of the seismic performance of an advanced elastoplastic sand constitutive model on a boundary value problem including kinematic and inertial soil-structure interaction. The results of the finite element numerical model for the free field and structural responses are compared with the experimental work on a group of piles analysed in a flexible soil container filled with dry sand and subjected to simplified seismic loading. In general, the comparisons show a satisfactory match between the results of the simulations and the experiments, with the exception of the numerical predictions of settlements. The computed results are discussed based on: i) the dominant stress-paths in soil; ii) parametric studies on the settlement evaluation; iii) the origin of the high frequency motion oscillations to simple sinusoidal input motions; all with respect to potential improvements in the formulation of the elastic behaviour of the constitutive model in the future.

https://doi.org/10.5459/bnzsee.1667

INTRODUCTION

Comprehensive understanding of nonlinear soil behaviour and soil-structure interaction (SSI) is of paramount importance for resilient societies of the future. Soil behaviour and SSI under seismic and, more recently, offshore loading conditions have been widely studied (e.g. [1,2] and [3,4], respectively). The origin of SSI under seismic loading comes from the fact that soil causes a structure to vibrate, and the vibrating structure in response affects the surrounding soil. The SSI can be split into kinematic interaction, when a structure has stiffness but no mass, and inertial interaction, when the structure has also the mass which affects the motion of the surrounding soil as (e.g. [5,6]). Although generally the SSI effects have been acknowledged, with analytical approaches approximating the solution through superposition of the kinematic and inertial effects, further advanced experimental and numerical studies follow in order to detail the knowledge on SSI and allow improved predictions of the response of real structures to seismic loading.

Small scale physical modelling is one of the approaches to study the dynamic behaviour of soil and SSI and, subsequently, to allow validation of numerical studies. Numerous experimental studies have been carried out in the recent past, including those dedicated to earthquake loading conditions, either in a 1g stress state (e.g. [6-10]) or centrifuge (e.g. [11-14]). In addition to the small-scale experimental tests, less common large-scale experiments on seismic SSI have also been conducted (e.g. [15,16]).

Numerical modelling, such as the finite element method, is a powerful tool to study seismic soil behaviour and SSI, and it is an attractive alternative to physical modelling. Robust advanced soil constitutive models capable of simulating soil cyclic nonlinear behaviour are needed to carry out reliable predictions in numerical studies. There is a vast number of advanced soil constitutive models developed within the classical elastoplasticity which have been shown to be able to replicate soil cyclic behaviour (e.g. [17-25]), thus they were indicated to be good candidates to be used in the seismic analysis of boundary value problems. A different family of soil constitutive models successfully dealing with soil cyclic loading is based on the hypoplasticity theory (e.g. [26,27]). The hypoplastic models for sands [28,29] and their developments to account for the small strain stiffness [30] and the reduction in the accumulation of strains in loading cycles [31,32] are well-recognized in soil numerical modelling.

The two families of constitutive approaches and the above-mentioned constitutive models are not the only candidates to simulate soil cyclic behaviour. For example, [33] presented a constitutive model based on the approach of nested yield surfaces showing its implementation to be successful in replicating sand cyclic behaviour. In fact, the number of available soil constitutive models is greater and is still growing. On the other hand, although attempted for some models in certain aspects, detailed validation of the available advanced soil constitutive models regarding their accuracy in modelling boundary value problems, in particular on seismic SSI, is still rather rare. Some advanced soil constitutive models have been shown to replicate cyclic element tests successfully, subsequently have been implemented in finite element codes and used to make predictions for boundary value problems (e.g. [34-36]). Nevertheless, ideally before the constitutive models are used in predictive studies, another important step in the validation of soil constitutive models is their ability to replicate experimental data regarding complex boundary value problems, including large soil domains of varying characteristics and different types of SSI.

Some previous research has been dedicated to the validation of soil constitutive models based on comparisons of numerical predictions with benchmark experimental works in flexible soil

[1] *Research Fellow, University of Southampton, Southampton (UK), p.kowalczyk@soton.ac.uk*

containers. One of the first such studies [37] used a simple Mohr Coulomb model and an advanced Pastor-Zienkiewicz constitutive model [38] to simulate the shear stack tests of Dar [39]. The authors indicated a need to develop more reliable soil constitutive models, in particular models able to account for dependency of strength and dilatancy on the mean effective pressure. Similar conclusions were also found by others [40,41] when using simple constitutive models. A large number of codes were verified in PRENOLIN (PREdiction of NOn-LINear soil behaviour) project which dealt with nonlinear site response [42]. The authors concluded that the numerous tested numerical tools were not consistent with each other and showed a significant misfit with the measured observations of the site response. A different study [43] summarized results of five different predicting teams in the numerical round robin competition for the seismic simulations of a tunnel embedded in dry granular soil [11]. All teams were able to fairly well reproduce acceleration records in free field, both, in terms of the amplitudes and the frequency content. On the other hand, a consistent trend of underestimated settlement was shown by all five teams and the representation of the bending moments and hoop forces in the embedded tunnel was captured only to a qualitative point. In addition to the mentioned studies, selected advanced soil constitutive models were validated during the series of the LEAP projects. The summary of the numerical predictions for the LEAP-2017 [44] showed that various numerical codes performed generally well; however, some inconsistencies were still found in the site response of a sloping ground (no SSI was analysed). In addition to [44], more detailed studies were shown by all the teams participating in the LEAP-2017 project. For instance, [45] used the well-known SANISAND model [19] to model the site response and indicated that this soil constitutive model was capable to represent many aspects of saturated soil under seismic loading, but consideration of soil-structure interaction was again missing in this validation.

To sum up, there is a substantial number of soil constitutive models aimed at simulating soil cyclic behaviour. Nevertheless, only a limited number of them have been implemented in the commercial finite element codes and used to analyse large boundary value problems studied previously in benchmark experimental works, with comparisons including soil-structure interaction and structural response being rare. Therefore, there is a strong need for further validation studies on the performance of soil constitutive models, especially when involving soil-structure interaction under seismic loading conditions, to suggest potential changes in the model formulation and to allow the use of those models in predictive research works and in engineering practise.

The work presented in this paper shows a short validation study on the performance of an advanced elastoplastic soil constitutive model, namely the Severn-Trent sand model in its most updated version [46] when simulating soil response together with the kinematic and inertial SSI. The validation is carried out on examples of a benchmark experimental work on the seismic soil-structure interaction of piles in dry soil [47]. Importantly, it is the first attempted validation of the Severn-Trent sand model in the version proposed in [46] for the case of cyclic loading, which is of paramount importance prior to adopting this soil constitutive model to reliable design and predicting tasks in seismic engineering in the future. The results section presents comparisons of the numerical simulations and experimental results for two input motions and two different pile head conditions, including an experimental setup with a single degree of freedom (SDOF) structure on the top of one of the piles. Subsequently, the computational results are followed by short comments on three aspects of the soil dynamic response to cyclic loading with the aim of suggesting potential improvements in the formulation of the constitutive model. Firstly, the most important stress paths computed in the numerical study are discussed with respect to potential improvements in the numerical computations if elastoplastic coupling was introduced in the formulation of the elastic law. Secondly, the inconsistencies in the predicted settlements are detailed based on the parametric studies on selected model parameters in regard to the need of introducing nonlinearity of a hysteresis shape in the elastic region. Finally, the origins of the high frequency oscillations computed in the numerical studies and measured in the experimental work are briefly discussed regarding the release of soil elastic waves in nonlinear hysteretic soil as identified in recent works [48-50] and potential future research developments in soil constitutive modelling.

METHODOLOGY

This section presents details of the benchmark experimental work from literature [47] adopted in this study and used to validate the soil constitutive model. The finite element model is described in the subsequent section.

Benchmark Experimental Work on Soil-Structure Interaction

Introduction to Experiments in Flexible Soil Containers

The experimental work in a flexible soil container at a 1-g stress level used in this work as a benchmark experimental reference for the numerical study was summarized in previous research works ([6, 9, 10, 47]). The currently used soil container [51] consists of eight aluminium stacks put on top of each other with flexible rubber links in between in order to allow soil to control the mechanical response in the soil-shear stack system subjected to shaking. The shear stack dimensions are: 1200mm length, 800mm height and 650mm width. The scaling laws between an experimental model and a real size prototype were given by Muir Wood et al. [7] and are not recalled here.

Soil Profile

The experimental work [47] was carried out with Leighton Buzzard sand dry pluviated in the shear stack. Two different fractions of this sand were used, namely fraction E in the top ‘softer’ Layer A and a mixture of fractions B (85%) and E (15%) in the bottom ‘stiffer’ Layer B resulting in a soil specimen characterised by the first natural frequency of around 25-30 Hz depending on the amplitude of the input motion [47]. The properties of the sand layers in the shear stack are presented in Table 1.

Pile and Structure Modelling

The experimental work comprised a five-pile group with different pile head conditions, including free-head piles, a short cap spanning the three closer piles (piles no. 1, 2 and 3), and a long cap spanning all five piles, all to simulate the kinematic soil-structure interaction. In addition, some experimental runs included a SDOF oscillator placed on the pile no.3 in order to simulate a structure and study the inertial soil-structure interaction. The piles were installed before the soil was pluviated into the soil container, thus can be considered as ‘wished-in-place’. The experimental setups for two cases analysed numerically are shown in Figure 1. The pile model was an aluminium tube of 750mm length, 22mm external diameter and 0.71mm wall thickness. The piles on their tops were equipped with a plastic cap with instrumentation (accelerometers, transducers) of a total mass approximated in this paper to be around 80grams. The structure was modelled as a 100mm long aluminium column of a rectangular section 3mm x 12mm and a variable mass on the top of the column to simulate the behaviour of a SDOF oscillator.

Table 1: Properties of Leighton Buzzard sand within two soil layers modelled in the experiment by Durante [47].

	Layer A	Layer B
Sand type	Leighton Buzzard, fract. E	Leighton Buzzard, fract. B +E
Dry density, ρ_d [kg/m^3]	1332	1800
Void ratio, e [-]	0.91	0.48
Relative density, D_r [%]	26	41
Specific gravity, G_s [-]	2.647	2.647
Minimum void ratio, e_{min} [-]	0.613	0.289
Maximum void ratio, e_{max} [-]	1.014	0.614
10% percentile, D_{10} [mm]	0.095	-
50% percentile, D_{50} [mm]	0.14	-
Reference	[52]	[53]

Monitoring Instruments

The monitoring instrumentation included accelerometers, displacement transducers, strain gauges and an Indikon instrument to measure the settlement. The placement of the part of the instrumentation from the experimental setup used in the result presentation of this paper is shown in Figure 1. The details of all the data measurement channels are available in [47].

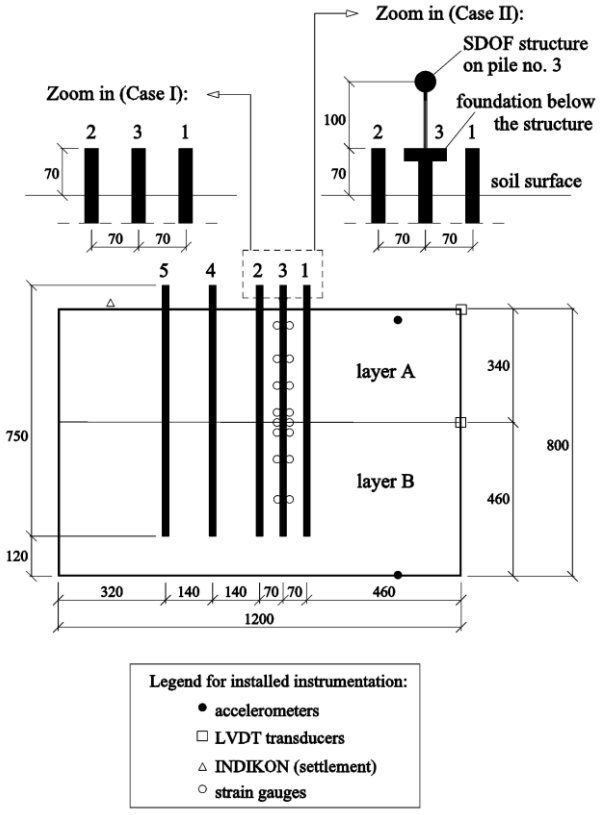

Figure 1: Geometry of 1-g experimental setup, part of monitoring instrumentation and pile numbering of pile group in shear stack as per Durante [47] for the two analysed cases (dimensions in mm).

Some of the measuring channels in the experiment were a subject to a filtering procedure (to the best of the Author's knowledge by means of a lowpass Butterworth filter 80Hz, 5th order) in order to reduce the experimental noise [47].

Input Motions

Two out of seven input acceleration time histories of moderate amplitudes analysed by the author in the past [48] have been chosen in this study (note that the general conclusions on the reliability of the constitutive model are not dependent on this choice). The sinusoidal input motions and the pile head conditions analysed in this paper in Case I and Case II are shown in Table 2. The experimentally and numerically applied input motions were introduced as sinusoidal cycles of a steadily growing amplitude. Note that there is some slight difference in the amplitude of the first few cycles before the part of the constant amplitude of motion is reached, since the primary focus of the study was the latter part of the motion of the constant amplitude. In fact, a different work [50] showed explicitly that soil nonlinear response under similar sinusoidal input motions does not depend on how the loading is introduced in first cycles. Both cases of input motions shown in Table 2 comprise the free-head pile (FHP) condition. The second analysed input motion is for the case of the pile no. 3 with a single degree of freedom (SDOF) oscillator on the pile top. The numerical analyses in this paper have focused solely on S-wave propagation, therefore accelerations throughout this paper should be explicitly understood as horizontal accelerations.

Table 2: Selected input motions and pile head conditions.

	Case I	Case II
Type	sinusoidal	sinusoidal
Frequency, f_{input} [Hz]	25	10
Max. acceleration, a_{max} [g]	0.77	0.155
Pile head conditions [-]	FHP	FHP+SDOF

Finite Element Model

This section presents the finite element model carried out in Abaqus [54] including a brief presentation of the soil constitutive model, its calibration and the geometry of the model.

Soil Constitutive Model

The soil constitutive model used in this work belongs to the family of elastoplastic soil models. Its current formulation [46] and implementation [55] is a development of the Severn-Trent model [17,18]. The original formulation of the Severn-Trent model [17,18] was based on the bounding surface approach and showed a constitutive model capable of accounting for the well-known geotechnical concepts such as the critical state, the Mohr-Coulomb failure and the current density and pressure measure in the form of the state parameter Ψ [56].

The updated version of the Severn-Trent model used in this work [46] was formulated within the kinematic hardening elastoplasticity, however resulting in an equivalent formulation to the boundary surface approach [17,18]. In [46] the flow rule of the original model was updated to improve the predictions of the volumetric compression observed typically under load reversals in cyclic loading. The updated flow rule linking the volumetric plastic deformation with the distortion shear strains was expressed as follows [46]:

$$\frac{tr\boldsymbol{P}}{\|dev\boldsymbol{P}\|} = -\frac{\sqrt{3}}{\sqrt{2}} A \frac{1}{g(\Theta_{(\sigma)})p}[(1 + k_d\psi) dev\overline{\boldsymbol{\sigma}_c} - dev\boldsymbol{\sigma}] \cdot \frac{dev\boldsymbol{Q}}{\|dev\boldsymbol{Q}\|} \quad (1)$$

Where $\boldsymbol{P}$ is the plastic flow direction, $\boldsymbol{Q}$ is the gradient of the yield surface, $g(\Theta(\sigma))$ is a function of a Lode's angle $\Theta(\sigma)$, $\overline{\boldsymbol{\sigma}_c}$ is the conjugate stress tensor in the normalized stress space, p is the mean stress p= -tr $\boldsymbol{\sigma}$/3, Ψ is the state parameter [56], A and k_d are the model parameters controlling volumetric response.

The plastic stiffness was defined as depending on the distance from the strength surface and on the Lode's angle in the deviatoric plane, thus two plastic stiffness parameters were needed (B_{min} and B_{max}). In addition, a 'smoothening' model parameter α was introduced to ensure a smooth stiffness change between the elastic and the plastic stiffnesses.

The most prominent feature of the updated formulation is a hyperelastic law within the yield surface instead of the previously used simplified hypoelastic formulation. This hyperelastic formulation presented first in [57] was the first one to account simultaneously for the changes in void ratio and the stress level on elastic anisotropy. Therefore, it was expected to correctly simulate all aspects of the small-strain behaviour of granular materials and to be "elasticity everybody wanted" [46]. In contrast, hypoelasticity, although often used in constitutive modelling in soil elastoplastic models, is not thermodynamically consistent, i.e. it can predict unclosed stress-strain loops, thus generating energy in the analysed system and may yield unreliable predictions. Instead of using a hypoelastic law, in [46] the nonlinear elastic law was derived from the free energy density function φ:

$$\varphi(\boldsymbol{\varepsilon^e}, \boldsymbol{\varepsilon^p}) = \gamma d\left(-tr(\boldsymbol{B}\boldsymbol{\varepsilon}^e)\right)^{\eta} + \zeta d(tr(\boldsymbol{B}\boldsymbol{\varepsilon}^e)^2)^{\lambda} \quad (2)$$

where: $\boldsymbol{\varepsilon^e}$ is the elastic strain, $\boldsymbol{\varepsilon^p}$ is the plastic strain, $\boldsymbol{B}$ is a fabric tensor (symmetric, second-order, positive-definite and dependent on plastic strain $\boldsymbol{\varepsilon^p}$) and d, γ, η, λ and ζ are constitutive parameters. In the original formulation tensor $\boldsymbol{B}$ describes the developing fabric anisotropy due to plastic strains (i.e. elastoplastic coupling). The model implementation used herein [55] has been simplified to facilitate the numerical convergence, i.e. tensor $\boldsymbol{B}$ is kept constant with no initial anisotropy specified and the changes in anisotropy due to plastic strains are not accounted for. This simplification in the implementation is discussed later in the text when suggesting potential improvements in the numerical predictions. More details regarding the formulation of the Severn-Trent model can be found in the referenced works [17,18,46].

Note that the constitutive model was shown to replicate soil element tests carried out at various mean effective stresses (including p' as low as 20kPa) with a single set of calibrated parameters [46]. Therefore, (although some uncertainties due to the effect of scaling in the experiment are unavoidable) the model can be expected to yield reliable predictions for an experiment carried out in the 1g stress condition.

To sum up, the Severn-Trent model in its current version is one of the most innovative constitutive approaches, which, however, has not been validated on a boundary value problem involving cyclic loading. Therefore, the presented work addresses this gap by investigating the performance of the model regarding replicating the dynamic behaviour of soil and seismic kinematic and inertial SSI.

Calibration of the Constitutive Model

No laboratory work on the small strain shear stiffness of Leighton Buzzard sand (fraction E & fraction B+E) at low mean effective stresses is known to the author. As a result of this, the calibration of the constitutive model has been based on the G/G_0 stiffness degradation derived for the simple shear deformation in dry sands at low mean effective stresses in similar shear stack studies [58]. Figure 2 shows the G/G_0 curves predicted by the constitutive model when evaluated at low mean effective pressure in simple shear tests. Generally, the calibration of the constitutive model fits well within the limits specified in [59] and remains close to the G/G_0 curves established by others (i.e. [58,60]).

Therefore, such choice for the calibration of the constitutive models can be deemed suitable in the light of no specific soil element laboratory works on Leighton Buzzard sand. Note that the simulations presented in this work are of class C according to the classification in [61], i.e. as per the case when the experimental results are known before calibrating the numerical model.

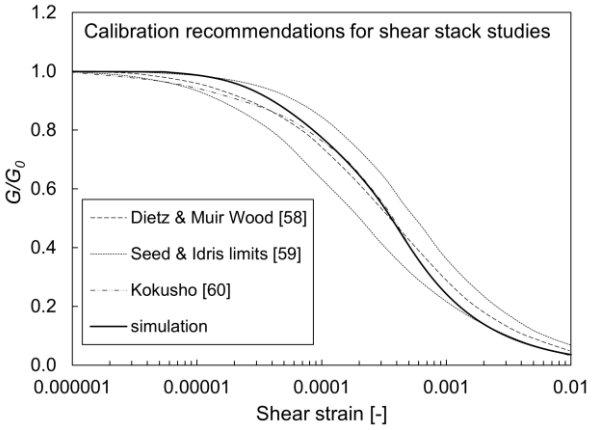

Figure 2: Calibration recommendations for constitutive models in shear stack studies given in terms of stiffness degradation behaviour G/G_0.

The calibrated model parameters are listed in Table 3. The performance of the constitutive model with this set of input parameters and an adjusted void ratio (i.e. 0.9 instead of 0.756) to model different sand is shown in Figure 3 when simulating an experimental laboratory test on Toyoura sand [62]. When replicating this test, the 'shakedown' is reached sooner in the numerical computations than in the experiment, however, the constitutive model is shown to capture the compressive behaviour. The increase in the tangent stiffness has not been fully captured (i.e. overestimated at very small strains, underestimated at larger strains). Nevertheless, the slight increase in the strength and the secant stiffness observed with the consecutive loading cycles is well captured when simulating the cyclic simple shear test at the strain level of up to 3%.

Note that the two soil layers A and B in the shear stack experiments have been modelled using the same set of model input parameters. The only difference between the two layers lied in: a) the void ratio which has been chosen to be 0.91 (Layer A) and 0.85 (Layer B) in order to achieve relative densities of 26% and 41% as per the experiments (Table 1), b) the dry density of soil (also as per Table 1). Although such modelling approach is a simplification it was shown in the past to be successful in the case of simulating different sands with a single set of model parameters and an equivalent void ratio (e.g. for Hostun and Toyoura sands [46]).

Soil Geometry, Boundary Conditions and Discretization

The finite element analysis was run in two phases. Firstly, a geostatic stage was run to ensure the initial stress state was in equilibrium with the gravity loading and resulting in negligible strains, i.e. to be representative of the experimental setup. The

lateral stress coefficient K_0 has been assumed to be 0.5 as expected to be the case when dry pluviation was used in filling the soil container [47]. The boundary conditions in the geostatic stage included restricting the vertical displacement at the base and the horizontal displacements on the four sides of the soil specimen to account for the presence of the soil container, whereas the vertical displacements on the sides were left unrestricted to allow application of the gravity loading.

Table 3: Input model parameters of the constitutive model.

Parameter	Role of the parameter	Value
v_Δ	Intercept for critical-state line in v-ln p plane at p=1Pa	2.194
Δ	Slope of critical-state line in v-ln p plane	0.0267
φ_{cv}	Critical-state angle of friction	33°
m	Parameter controlling deviatoric section of yield surface	0.8
k	Link between changes in state parameter and current size of yield surface	3.5
A	Multiplier in flow rule	0.75
k_d	State parameter contribution in flow rule	1.3
B_{min}	Parameter controlling hyperbolic stiffness relationship for various stress paths in deviatoric plane	0.0005
B_{max}	Parameter controlling hyperbolic stiffness relationship for various stress paths in deviatoric plane	0.002
α	Exponent controlling hyperbolic stiffness relationship	1.6
R_r	Size of yield surface with respect to strength surface	0.02/0.01*
E_r	Fraction of G_0 used in computations	1.0**

** slightly larger yield surface has been assumed in Layer A to avoid numerical problems at shallow depths in the region of very low mean effective pressures*

*** equivalent value to 1.0 has been used in the input to ensure the initial elastic stiffness of G_0 captured the empirical evaluation [63] as aimed originally in [46]*

Boundary conditions on the two short lateral sides of the mesh have been redefined in the dynamic phase of the loading to tie connectors between the side nodes at the corresponding heights. Two approaches are typical when linking the nodes on the opposite sides, one restricting the horizontal and vertical degrees of freedom at the corresponding nodes (e.g. [37]), and second, probably more common, assuming constraining the corresponding nodes on both sides to the same horizontal displacement (e.g. [40]). The latter approach allows the vertical movement on both sides to differ and to account for the propagation of the surface waves induced by structural elements. In fact, the author in his previous work [48] constrained all degrees of freedom as inspired by [37] and since the experimental data [47] identified unaffected response in the free field and no presence of horizontally propagating surface waves. Instead in this work, the second approach was chosen as possibly more widely accepted among the geotechnical research community. In any case, this choice does not significantly affect the results of the validation of the constitutive model, as one can see by the comparisons of the results reported in this work with the results presented in [48].

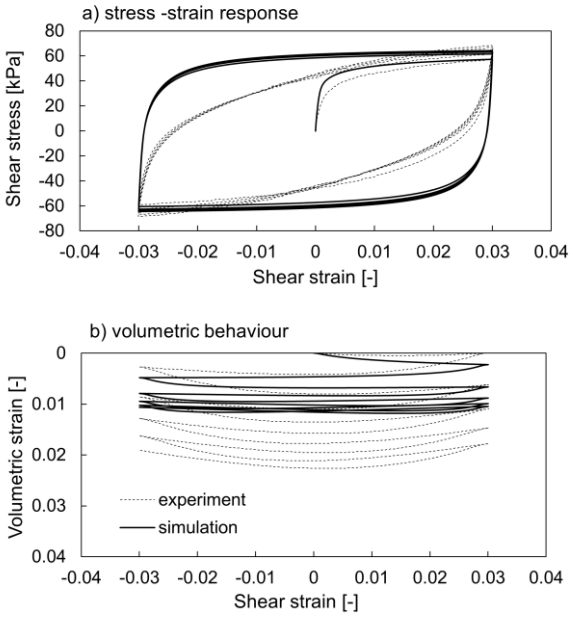

Figure 3: Comparison of simulations and experimental measurements of cyclic simple shear test on Toyoura sand at p'=100kPa (Shahnazari & Towhata [62]): a) stress -strain response, b) volumetric behaviour.

The seismic input motions have been applied as an acceleration time history of a single sine frequency (i.e. 'perfectly sinusoidal') at the bottom of the mesh. Therefore, the input motions applied in the numerical studies were slightly different from the recorded input motions (which contained a fractional number of higher harmonics). This permitted to investigate the ability of the hysteresis predicted by the constitutive model to generate high frequency motion. No dissipative boundaries have been defined at the bottom of the mesh as wave reflection is expected to be experienced in the shear stack placed on a rigid shaking table. The effect of the aluminium stacks has been omitted as typically considered of negligible influence [37,57] and sensitivity studies on the explicit modelling of the soil container were out of the scope of this study.

The element type for soil is a quadratic 'brick' element from the library of Abaqus elements [54]. The element size has been calculated from the elastic wave propagation for the slowest wave (i.e. G_0 of around 3MPa in the superficial soil) and the highest frequency (80Hz to account for the most important higher frequencies). This resulted in a maximum distance between two nodes to be 0.06m, which has been subsequently reduced to 0.025m (quadratic element size 0.05m) in order to account for nonlinearity developing in soil at shallower depths, and, therefore slower waves propagating as advised in [64]. Moreover, the ratio of the element size to the pile diameter remains within the limits of similar finite element numerical studies [34]. The optimal mesh together with the reference elements selected for the result presentation is presented in Figure 4. Due to the symmetry in the model, only a half of the shear stack has been modelled in order to reduce the computational costs.

The numerical results for the computed accelerations have been filtered, i.e. a lowpass Butterworth filter 80Hz (5th order) with a zero-phase shift has been used for the sake of consistency with the experimental data and to remove very high frequency numerical oscillations.

Pile Geometry and Discretization

Piles have been modelled as halves of the tubular piles. A shell element type has been chosen to model the tubular piles of a 22mm diameter and 0.71mm wall thickness. The piles have been modelled with a linear elastic material representative of aluminium, i.e. with stiffness E=70GPa and Poisson's ratio ν=0.3.

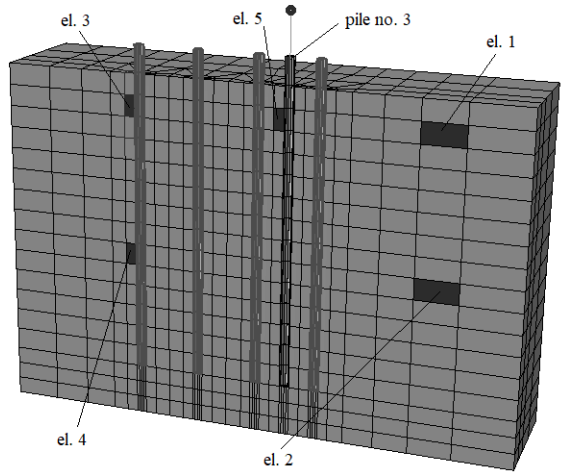

Figure 4: 3D mesh discretization for Case II (Table 2) with selected reference elements for presentation of results.

The soil-pile interface has been defined as frictional with an allowance for a gap opening. The coefficient of friction has been assumed to be 0.5 which is a typical value measured between granular soil and steel piles (e.g. [65]) and the parametric studies on the type of the interface were out of the scope of this study.

In addition, a mass of 80 grams has been modelled at the top of the piles in order to account approximately for the mass of an accelerometer and a plastic cap present in the experimental setup.

Oscillator Geometry and Discretization

The single degree of freedom oscillator has been modelled in Case II as a 100mm long column of aluminium material (see Figure 1), with a mass of 190 grams at the top (to simulate the oscillator mass) and a mass of 176 grams at the bottom (to simulate the foundation mass). Note that the foundation at the bottom was placed without contact with soil (as shown in Figure 1). The fixed-base natural frequency of such oscillator is 26.5Hz as assessed experimentally before [47]. Note that both masses were input as halves of the indicated values due to the fact of modelling only a half of the shear stack. The oscillator has been discretized with a beam element type of a rectangular aluminium section 3x6mm (half of the actual size 3x12mm) to be representative of the experimental setup [47].

RESULTS OF NUMERICAL SIMULATIONS

The numerical results compared with the experimental measurements are presented in two sections depending on the applied input motion (Case I and Case II). The results for the pile are referred to the pile no.3 within the five-pile group (see Figure 1 and Figure 4). The two sections are followed by short comments on three aspects of the dynamic response of soil to cyclic loading in order to suggest potential improvements in the formulation of the constitutive model.

Case I: Free-Head Piles without Oscillator

A comparison of the numerical and experimental results for Case I of the 25Hz input motion with the maximum input amplitude of 0.077g is presented in this section.

The response in free field in terms of the computed horizontal accelerations (Figure 5) and lateral relative displacements (Figure 6) is generally well simulated by the constitutive model, in particular in the part of the motion of the constant amplitude. The computed accelerations capture very well the measured accelerations in terms of the amplitude (thus the amplification of motion) and, with some very slight discrepancy, the phase shift between the input at the base and the motion at the top. Moreover, a distortion in the form of high frequency motion from the perfect sinusoidal input motion applied at the base can be clearly observed at the top of soil in the experiment and the simulation with only some mismatch in the distorted shape. The lateral relative displacements of soil are fairly accurately represented at two heights of the shear stack in terms of the amplitudes and the phase shifts. On the other hand, the computed settlements in the free field (Figure 7) reach up to 0.5mm and are overestimated in the simulations, even though the calibrated model was validated for the volumetric response to simple shear deformation (see Figure 3). Nevertheless, although the constitutive model overestimates settlement, on overall, this has a negligible effect on other computations. Additional parametric studies and comments on this difference between the experiment and the computations are shown later in the text of this work.

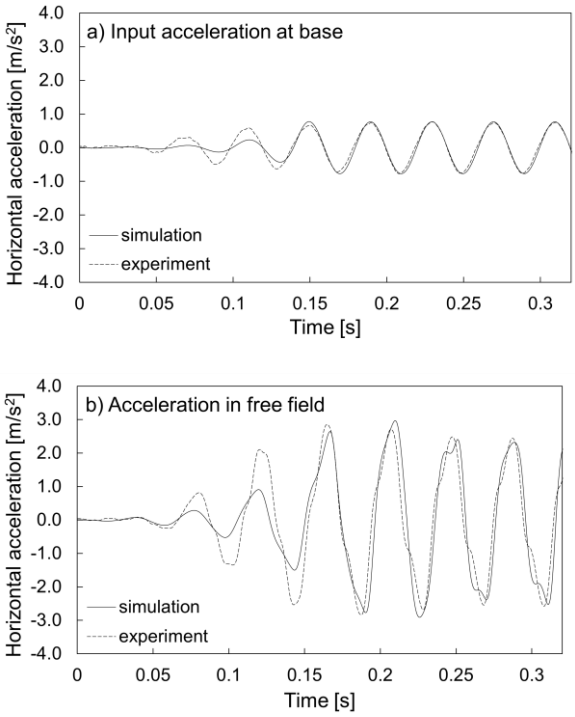

Figure 5: Comparison of: a) applied horizontal accelerations at base, b) measured and computed horizontal accelerations in free field at soil surface for Case I.

Regarding the pile response, the computed accelerations (Figure 8) match fairly well the experimental measurements in terms of the maximum amplitude in the part of the motion of the constant amplitude (i.e. from 0.15 sec). The constitutive model also indicates the presence of high frequency oscillations observed at the pile top in the experiment. This effect has been reasonably well captured in the simulations; however, the experimental measurements contain more prominent oscillations. More comments on the high frequency motion

computed and observed in soil and on the structural elements is given in a dedicated section later in the text.

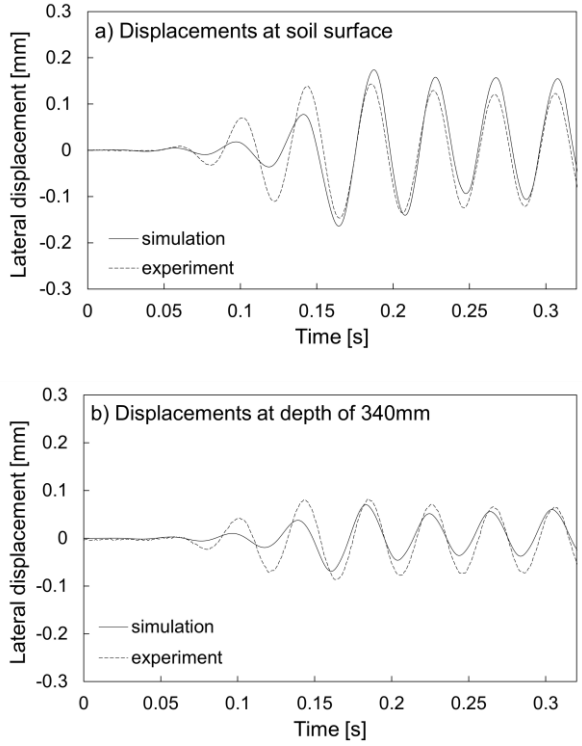

Figure 6: Comparison of measured and computed lateral relative displacements in free field in Case I: a) at soil surface level and b) at depth of 340mm.

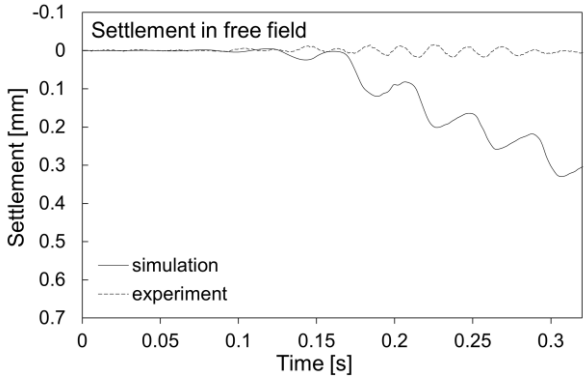

Figure 7: Comparison of measured and computed settlements at soil surface level in free field for Case I.

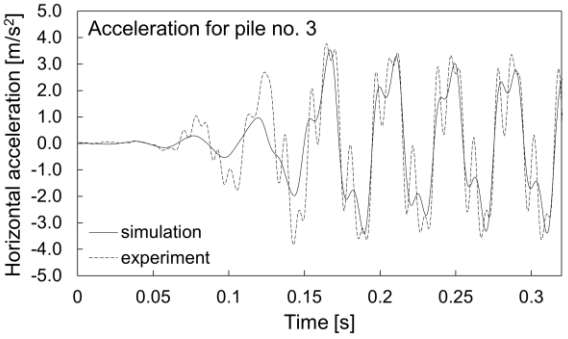

Figure 8: Comparison of measured and computed horizontal accelerations at top of pile no.3 for Case I.

Looking at the lateral relative displacements of the pile head (Figure 9) some inconsistency can be observed between the numerical prediction and the experimental measurement. Although the order of magnitude is maintained, the pile lateral displacements are underestimated in the numerical simulations. The reasons for this misfit have not been clearly identified; however it could be due to the approximate estimation of the mass of 80 grams (representing the plastic cap with measuring instrumentation) at the top of the piles in the numerical studies. Increasing this mass would lead to improvement in the computed response in Figure 9, however, would be more difficult to justify than the estimated mass of 80 grams, thus, parametric studies on this aspect of modelling were not considered.

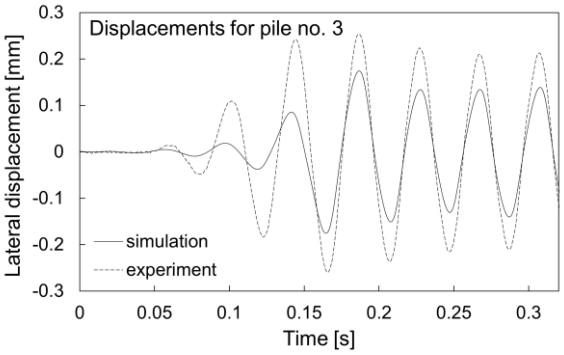

Figure 9: Comparison of measured and computed lateral relative displacements at top of pile no. 3 for Case I.

Finally, the pile maximum axial strains (representative of the pile maximum bending moments) are compared in Figure 10. The simulations predict slightly unsymmetric response possibly due to some ratcheting behaviour experienced in soil which is discussed more later in the text. Although, some discrepancies can be observed, in general, the computed values are within the order of the magnitude of the experimental measurements and at similar depth of around 375mm, i.e. close to the interface between Layers A and B, as expected for a pile kinematically driven by soil.

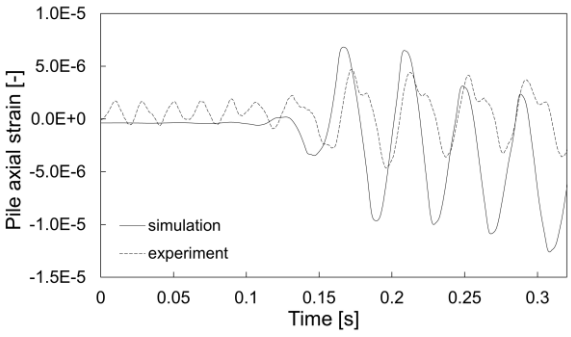

Figure 10: Comparison of measured and computed pile axial strains at depth of around 375mm for pile no. 3 for Case I.

Case II: Free-Head Piles with Oscillator

This section shows the results for Case II of the 10Hz sine input motion with the free-head pile conditions and a SDOF oscillator placed at the top of the pile no. 3.

Firstly, the response in the free field is compared (Figures 11-13). Generally, the accelerations in the free field (Figure 11) are matched well in terms of the computed amplitudes and with a slight discrepancy in terms of the phase shift (possibly due to different filtering techniques between experiments and simulations) when reaching the part of the motion with a constant amplitude. Note that the phase shift for the driving

frequency of 10Hz is less than for 25Hz with the amplification of motion being less than in Case I as expected, since the driving force of 10Hz is further away from the soil natural frequency (evaluated to be around 25-30Hz). The presence of high frequencies generated in soil is apparently overestimated in the simulations in this case. The computations replicate in a satisfactory manner the lateral relative displacement at the depth of 340mm and with some noticeable misfit at the soil surface level (Figure 12). The reason for the discrepancy at the top of soil could possibly be attributed to the presence of the flexible soil box not modelled explicitly in the numerical studies. On the other hand, the phase shift between the computed and the measured relative lateral displacement at the top of the soil has been captured accurately. The computed settlements in the free field (Figure 13) are again overestimated by the constitutive model. This modelling aspect is discussed in more detail in a dedicated section later in the text.

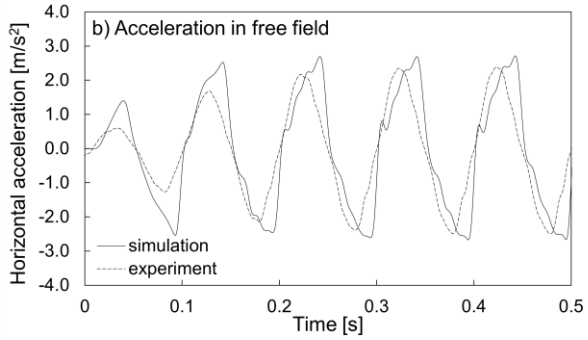

Figure 11: Comparison of: a) applied horizontal accelerations at base, b) measured and computed horizontal accelerations in free field at soil surface for Case II.

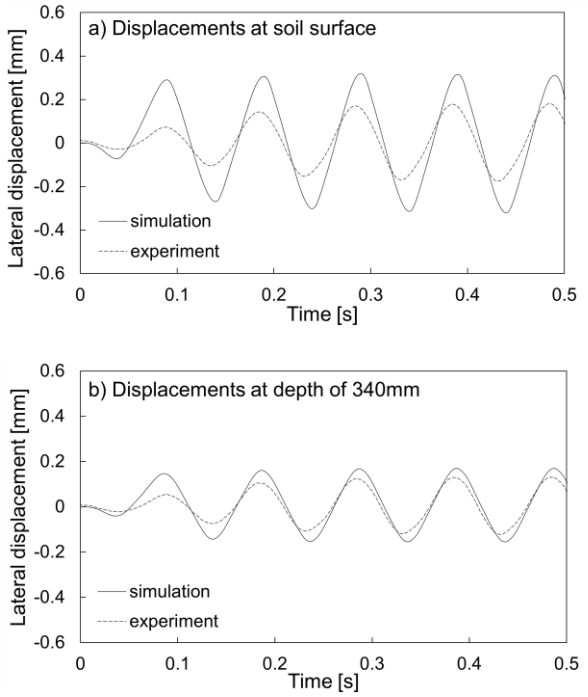

Figure 12: Comparison of measured and computed lateral displacements in free field for Case II: a) at soil surface level and b) at depth of 340mm.

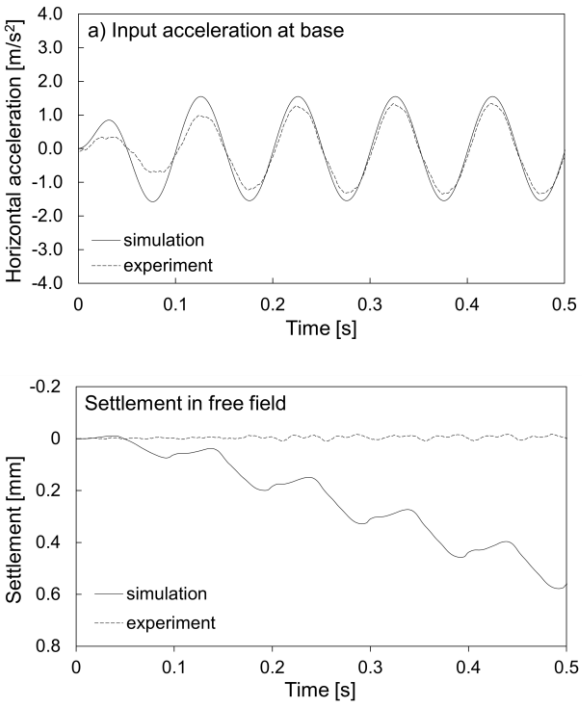

Figure 13: Comparison of measured and computed settlements at soil surface level in free field for Case II.

The horizontal accelerations of the pile no. 3 are shown in Figure 14 and are in fairly good agreement between the computations and the experiments, with stronger presence of high frequency motion oscillations in the numerical studies and a slight difference in terms of the simulated phase shift (similarly to the free field computations). The pile lateral relative displacements and the pile maximum axial strains are shown in Figures 15 and 16, respectively. The lateral relative displacements of the pile top match very well those measured in the experiment. This distinct difference in the match when compared with Case I (where a clear discrepancy has been pointed out) may be related to the fact that in Case II, the response of the pile is driven by the mass of the SDOF oscillator. In addition, to the correctly predicted amplitude, the computed and measured lateral displacements show a very slight distortion from the perfect sinusoidal motion, thus indicating again the presence of high frequencies. The maximum pile axial strains are measured and computed close to the top of the pile (at the depth of around 140mm) as expected for a pile with a structure on its top, with the numerical model overestimating slightly the amplitude of the measured axial strains (Figure 16).

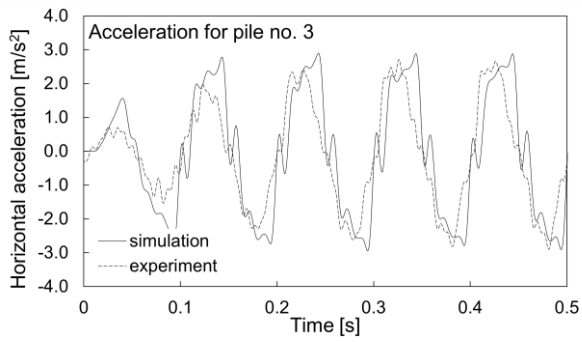

Figure 14: Comparison of measured and computed horizontal accelerations at top of pile no.3 for Case II.

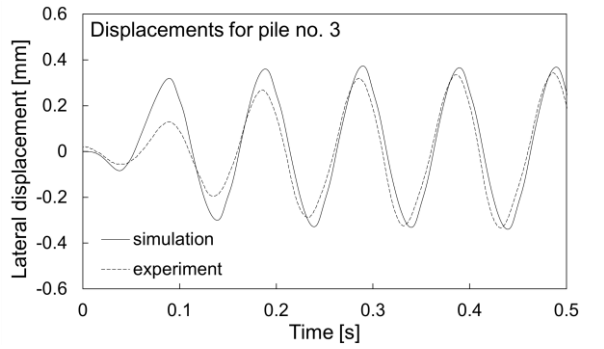

Figure 15: Comparison of measured and computed lateral relative displacements at top of pile no. 3 for Case II.

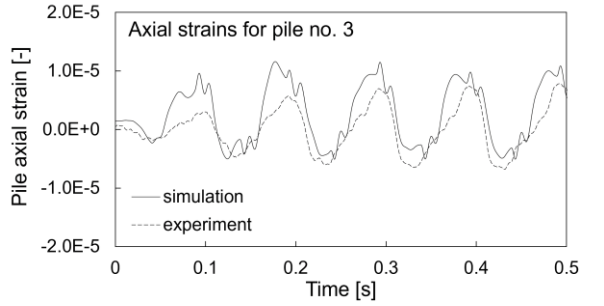

Figure 16: Comparison of measured and computed pile axial strains at depth of around 140mm for pile no. 3 for Case II.

Finally, the computed accelerations at the top of the SDOF oscillator show a satisfactory match with the maximum measured accelerations (Figure 17). Generally, high frequency oscillations are present in the motion of the oscillator in the numerical and experimental studies; although, their amount has not been captured very accurately in the simulations. Slightly overestimated phase shift in the computations is consistent with the simulations of the free field (Figure 11) and the accelerations computed at the top of the pile (Figure 14).

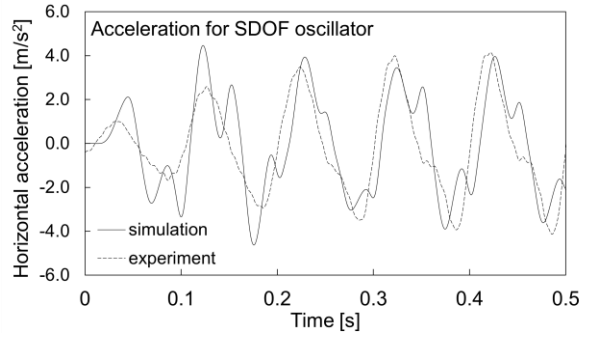

Figure 17: Comparison of measured and computed horizontal accelerations at top of oscillator for Case II.

In summary, the numerical predictions captured the majority of the experimental measurements with satisfactory accuracy for Case I and Case II. Nevertheless, some inconsistencies between the numerical and experimental results have been identified, thus suggesting that the formulation of the implemented constitutive model could be improved in some aspects. Some of those aspects are discussed in more detail in the next sections.

Stress Paths in Soil

This section presents the most representative stress-strain behaviours in the shear stack simulations in the selected five reference elements from the 3D mesh (Figure 4) in their middle Gauss points for the 10Hz sine input motion with the SDOF structure on the top of the pile no. 3 (Case II) in order to suggest potential improvements in the formulation of the constitutive model. The reference elements can be divided in three zones, representing the free field (elements no. 1 and 2), the vicinity of a pile under kinematic loading (elements no. 3 and 4) and the vicinity of a pile with a SDOF structure (element no. 5).

Figure 18 depicts curves of the shear stress normalized by the vertical effective stress τ/σ_v against the shear strain γ computed by the constitutive model for the five selected elements. Elements no. 1, 2 and partly element no. 4 (Figure 18a, b and d, respectively) show hysteretic fairly smooth behaviour almost as in simple shear tests, i.e. as expected in the free field or close to the pile but at depth where piles under kinematic loading are expected to be fully driven by the soil behaviour. On the other hand, elements no. 3 (Figure 19c) and especially no. 5 (Figure 19e) show more erratic stress strain curves. In these regions, the response is no longer dominated by the simple shear type of behaviour since the impact from the relatively stiffer pile with a smaller mass (element no. 3) or a larger mass (element no. 5) becomes dominant. Note that in some cases (e.g. element no. 4) it appears that the soil constitutive model predicts response with some accumulation of shear strains. Nevertheless, this 'ratcheting' behaviour apparently does not affect significantly the numerical computations when compared with the experimental measurements. In fact, some accumulation of shear strains would also be expected in the experiments.

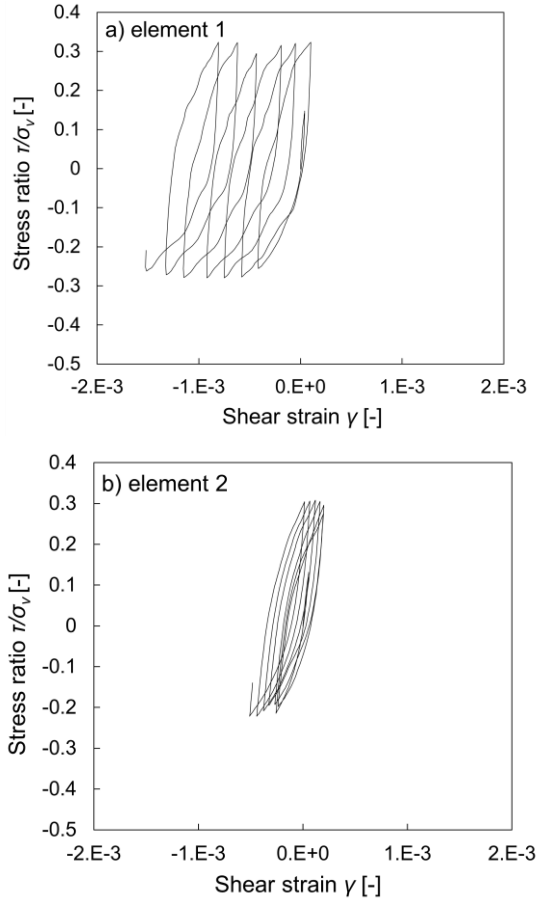

Figure 18 (continued in the next page): Shear stress-strain behaviour in: a) element no. 1 in free field at around 90mm depth, b) element no. 2 in free field at around 430mm depth.

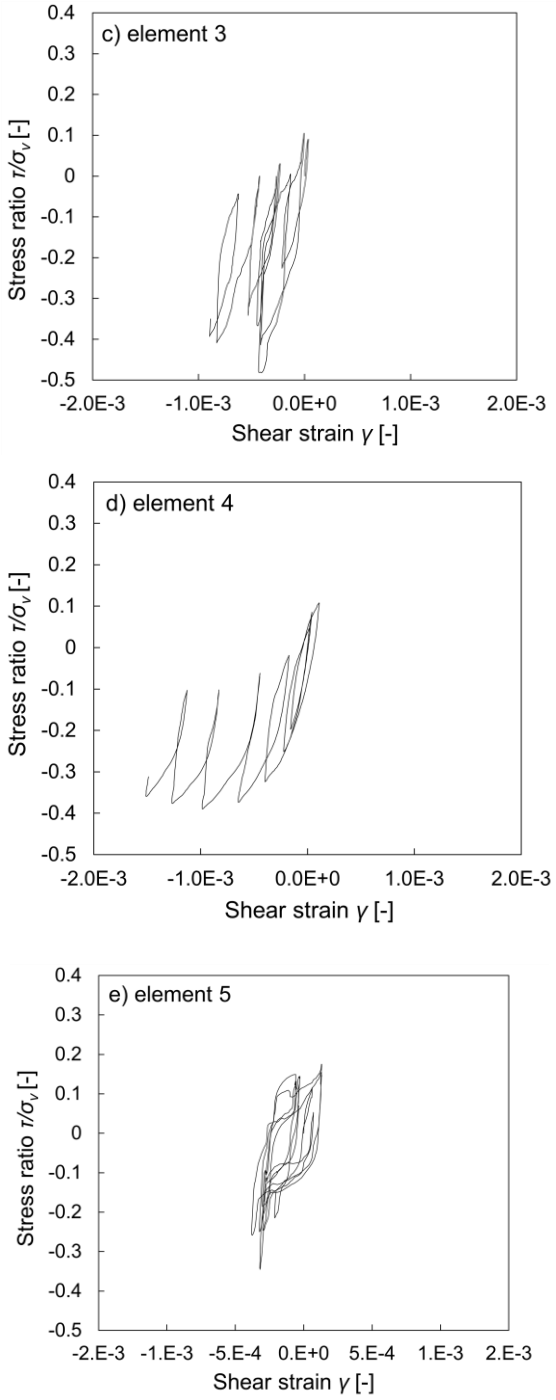

Figure 18 (continued from the previous page): Shear stress-strain behaviour in: c) element no. 3 in vicinity of kinematic pile at around 90mm depth, d) element no. 4 in vicinity of kinematic pile at around 430mm depth, e) element no. 5 in vicinity of kinematic pile with SDOF structure at around 90mm depth.

Figure 19 shows the lateral loading in terms of the stress ratio σ_h/σ_v versus the lateral strain ε_h on soil elements 1 and 5, respectively. The σ_h in the stress ratio is to be understood as the horizontal stress in the direction of the applied shaking (similarly the lateral strain ε_h is the horizontal strain in the direction of the applied shaking). Based on the computed stress-strain behaviour, it can be observed that the lateral type of loading is of less importance in the free field (Figure 19a) but it can be of increased importance for the pile with the oscillator on its top (Figure 19b). Large variations in the stress ratio σ_h/σ_v would be expected to be potentially important when investigating the fabric effects on changes in the small strain stiffness, i.e. changes in the stiffness anisotropy. The computed variations in the stress ratio σ_h/σ_v from 0.3 up to 1.4 shown here (Figure 19b), come from the moderate-level input motion (i.e. the maximum of 0.155g) and would be expected to decrease below 0.3 and increase beyond 1.4 for higher intensity seismic events, for which the changes in the stiffness anisotropy would be expected to be even more prominent, as shown in experimental works in the past (e.g. [66]).

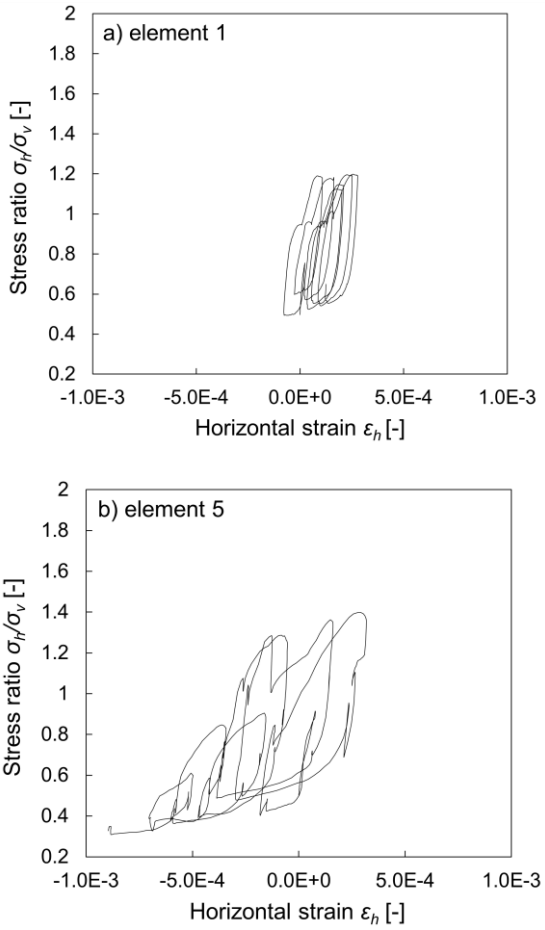

Figure 19: Stress ratio (σ_h/σ_v) versus horizontal axial strain curves for: a) element no. 1 at around 90mm depth, b) element no. 5 in vicinity of kinematic pile with SDOF structure at around 90mm depth.

Note that the computed and shown here stress strain curves apparently do not appear to be severely affected by 'overshooting' in the predictions of the soil stiffness and strength on reloading, i.e. a common limitation of many soil constitutive models, including the Severn-Trent model, as shown by the author previously [48, 67]. Nevertheless, it is admitted that the problem of 'overshooting' occasionally could also be encountered in the case of the boundary value problem analysed in this work.

To sum up this section, the future constitutive developments of the presented constitutive model could include features representative of the developing small strain stiffness anisotropy (e.g. such as in the original formulation [46]) which would be expected to improve the predictions of SSI.

Parametric Studies on Settlement Computations

The numerical computations for Case I and Case II have shown generally a satisfactory match with the majority of the experimental results apart from the predicted volumetric response, which was always overestimated by the constitutive model. This section presents parametric studies on the

numerical predictions of the settlements in the free field response exclusively (i.e. carried out in a simpler geometry of a soil column of the height of the soil specimen). To this aim, three model parameters were tested. The first two parameters are the flow rule parameters A and k_d (see eq. 1) and the third one is the yield surface size R_r. Figure 20a shows how the predictions of the settlement for Case I differ when parameters A and k_d are changed within their typical values (as listed in [48]) and compared with the model calibration (shown in Table 3 and in solid line in Figure 20). Apparently, regardless of the value of A and k_d the compressive behaviour is maintained, probably due to the fact that the soil is at loose relative density (D_r=25% at the top) which imposes its position versus the position of the critical state line, and thus, densification.

Alternatively to the changes in the flow rule, one could consider increasing the yield surface size to reduce the plastic volumetric deformation. In fact, in case of increasing R_r to 0.3, the volumetric deformations oscillate around 0 (as per the experiment), however, in this case the relative horizontal displacements at the top of the free field are much less satisfactory than when the small yield surface size is assumed (Figure 20b).

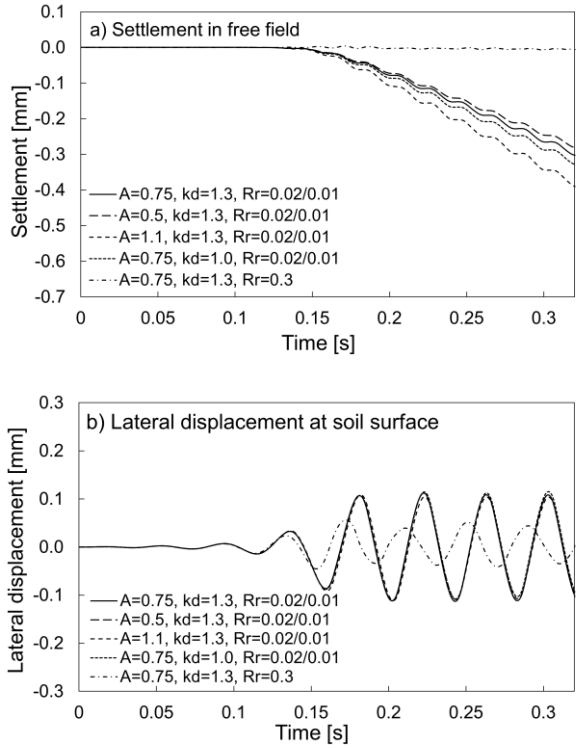

Figure 20: Parametric studies on variations in flow rule parameters A and k_d and yield surface size parameter R_r: a) predictions of settlement, b) predictions of relative lateral displacement.

In this point, it is worth to remind that some research works (e.g. [68,69]) identified two zones of soil elastic behaviour, linear elasticity and nonlinear hysteresis elasticity. Possibly including explicitly these two zones of elasticity in the constitutive model would allow to model together more accurately settlement (where plastic volumetric responses needs to be minimised) and lateral relative displacements (where hysteresis nonlinearity is needed) in the analysed experiment.

Origin of High Frequency Motion

This section makes some brief comments on the presence and the origin of the computed and measured high frequency motion oscillations in the dynamic response of soil and the structural elements.

The computations of the horizontal accelerations presented in this paper show clearly distortion from simple sinusoidal motions when inspecting the response in the free field in soil and, especially, on the piles. This is observed even though the applied input motions were perfectly sinusoidal when defined at the soil base in the numerical computations. In fact, even the experimentally applied input motions contained only a fractional (Case I) and a slightly higher, but still limited (Case II), number of higher harmonics with the dominant 'intrusive' frequency being 50Hz and representing the electric current. Figure 21 shows an example of the Fast Fourier Transform of the input motion and the free field response measured experimentally for Case I where the input motion was less affected by higher harmonics (FFT was evaluated for the part of the motion with the constant amplitude). The transfer function computed as a ratio between the spectral response of the measurements at the top to the input motion at the base shows amplification of the higher modes of the soil natural frequencies of 75Hz and 125Hz (Figure 21c). The evaluated amplification of high frequency motion at the frequencies of 75Hz and 125Hz is around 100 and, therefore, it cannot be easily justified by the linear elastic wave amplification theory (e.g. [70]), where the amplification ratio for the linear elastic soil would not be expected to exceed 20 in typical site responses [71]. The transfer function for the corresponding computations has not been plotted since the numerically introduced input motion is an ideal sinusoidal function (i.e. only the driving frequency of 25Hz is present in the input), thus the additional harmonics are apparently fully generated due to soil nonlinearity, as explained in more detail below.

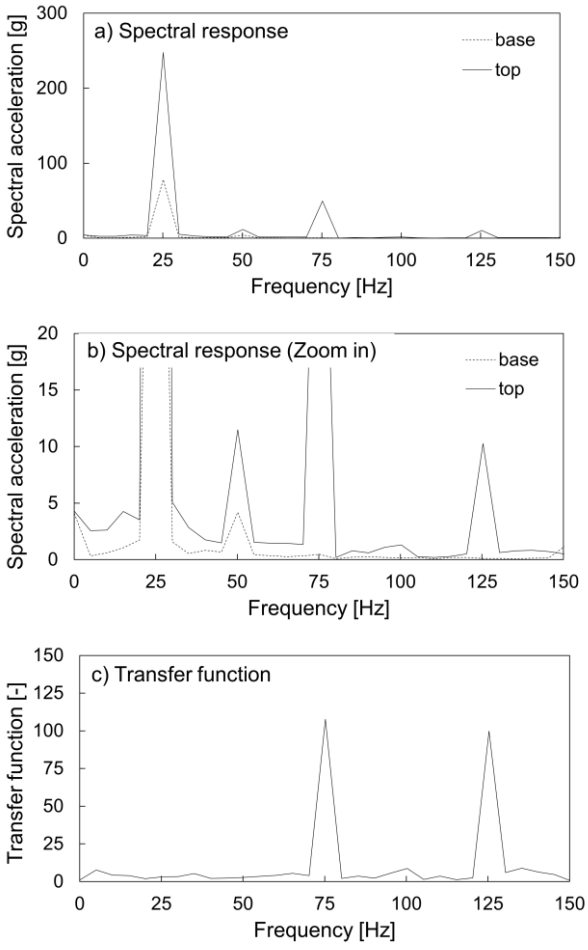

Figure 21: Spectral acceleration at top and base (a,b) and transfer function (c) for Case I.

The presence of high frequency motion was recently attributed to an unrecognized physical phenomena of soil elastic waves, firstly initially in [48], and subsequently in [50]. The latter work suggested potential gaps in the theory of wave propagation and showed how soil elastic waves can be released in soil modelled with a hysteretic-type nonlinearity (without consideration of plastic deformation). The soil elastic waves were identified as: i) soil natural vibrations and, ii) an elastic strain/strain discontinuity; both released in the soil modelled with a nonlinear hysteresis. The soil elastic waves were shown to lead to regular patterns of high frequency motion being observed when soil is subjected to simple sinusoidal input motions. Therefore, in the work presented herein, high frequency motion can be expected to be also representative of the soil elastic waves generated in nonlinear soil. Importantly, this work shows that such high frequency motion (although often of slightly different patterns) has been captured equally in the numerical and experimental results, including the response of the structural elements, thus affecting SSI. In general, such behaviour, when a pile or a structure appears to amplify the soil-generated high frequency motion, may even lead towards a resonance between the structural natural frequency with the soil elastic waves as shown in a different work of the author [49] which was developed based on the findings from [48,50].

Note that in the case of the benchmark experimental study [47] used herein, it is difficult to identify unanimously the actual origin of the high frequencies. There are some initial proofs [48-50] supporting the existence of soil elastic waves in experimental works. However, one should not forget that additional waves in the analysed experimentally system [47] could possibly be induced in other manners, for example as a result of wave reflections on the interface of the bi-layered soil profile, wave scattering from the piles, or impact of the boundaries, i.e. the interaction of soil with the soil container. Although numerical studies can clearly show that these characteristics of the experimental setup have a secondary effect to soil hysteresis when investigating the origin of high frequency motion, a clear experimental proof has not been obtained yet. Therefore, further research is needed, possibly with re-reviewing previous experimental works (e.g. [39]), proposing dedicated physical small-scale testing [72] or carrying out simpler experimental work on s-wave propagation [73] to clearly identify the origin of the high frequency motion in experimental works. Such works could unveil more on the soil mechanical behaviour to dynamic loading, including: i) clear determination of the actual soil elastic region (as suggested also in [48]), ii) guiding towards potential future improvements in soil constitutive modelling, e.g. the need for introducing different damping characteristics for soil-generated elastic waves from the incoming waves from a source, iii) improved understanding of the response of seismic sites such as Mexico City or Wainuiomata (NZ) characterised often by long-duration monochromatic vibrations (as briefly highlighted in [74]).

SUMMARY

This paper has presented the performance of the advanced sand constitutive model in the numerical modelling of the benchmark experimental work on the dynamic response of soil together with the kinematic and inertial soil-structure interaction. It has been shown that the investigated sand constitutive model is capable of simulating soil cyclic behaviour and soil-structure interaction in seismic applications in at least satisfactory manner, and in most cases with high accuracy, including the predictions in the free field and the response of the structural elements. Some inconsistencies in the numerical predictions have been identified and discussed with respect to the potential improvements in the formulation of the constitutive model. The suggested updates in the formulation have included:

- Accounting for elastoplastic coupling in the formulation of the elastic law to capture SSI more accurately in cases where the elastic stiffness degradation due to the developing anisotropy is expected (i.e. around the top of the pile, especially the pile with a mass).
- Accounting for the strain range of soil behaviour with elastic hysteresis (additional constitutive ingredient typically not appreciated in modelling soil dynamic response) to improve the predictions of the volumetric response without impacting on the remaining aspects of the dynamic response of soil.
- Speculations on potential new constitutive developments aimed at improved simulation of high frequency motion due to soil-released elastic waves (subject to confirmation of the results of dedicated experimental works).

ACKNOWLEDGMENTS

The research presented herein has been initiated under the XP-Resilience project. This project received funding from the European Union's Horizon 2020 research and innovation programme under the Marie Skłodowska-Curie grant agreement No 721816.

The author would like to thank Dr Maria Giovanna Durante (University of Calabria, Italy) and Professor Luigi Di Sarno (University of Liverpool, United Kingdom) for providing examples of raw experimental data of the benchmark experiments on soil-structure interaction. Special further thanks to Dr Maria Giovanna Durante for a brief but fruitful email exchange regarding experimental details.

The author acknowledges Professor Alessandro Gajo (University of Trento, Italy) for the provision of the numerical tools and some advice during the PhD research of the author where the work presented in this manuscript was commenced, and for some comments to the draft of this manuscript.

The author would also like to thank to an anonymous reviewer for valuable suggestions on adjustments to the manuscript.

The author acknowledges the use of the IRIDIS High Performance Computing Facility at the University of Southampton (UK), together with associated support services (in particular guidance from Dr Yifu Zhang) in the review stage of this work.

REFERENCES

1 Pitilakis D, Dietz M, Muir Wood D, Clouteau D and Modaressi A (2008). "Numerical simulation of dynamic soil-structure interaction in shaking table testing". *Soil Dynamics and Earthquake Engineering*, **28**: 453-467. https://doi.org/10.1016/j.soildyn.2007.07.011

2 Loli M, Apostolou M, Gazetas G, Gerolymos N and Anastasopoulos I (2010). "Soil failure can be used for seismic protection of structures". *Bulletin of Earthquake Engineering*, **8**: 309-326. https://doi.org/10.1007/s10518-009-9145-2

3 Zhou Z, O'Loughlin CD, White DJ and Stanier SA (2020). "Improvements in plate anchor capacity due to cyclic and maintained loads combined with consolidation". *Géotechnique*, **70**(8): 732-749. https://doi.org/10.1680/jgeot.19.TI.028

4 Cerfontaine B, White D, Kwa K, Gourvenec S, Knappett J, Brown M and Zhou Z (2023). "Anchor geotechnics for floating offshore wind: Current technologies and future innovations". *Ocean Engineering*, **279**: 114327. https://doi.org/10.1016/j.oceaneng.2023.114327

5 Mylonakis G, Nikolaou A and Gazetas G (1997). "Soil-pile-bridge seismic interaction: kinematic and inertial effects. Part I: soft soil". *Earthquake Engineering and Structural Dynamics*, **26**: 337-359. https://doi.org/10.1002/(SICI)1096-9845(199703)26:3<337::AID-EQE646>3.0.CO;2-D

6 Durante MG, Di Sarno L, Mylonakis G, Taylor CA and Simonelli AL (2016). "Soil-pile-structure interaction: experimental outcomes from shaking table tests". *Earthquake Engineering and Structural Dynamics*, **45**(7): 1041-1061. https://doi.org/10.1002/eqe.2694

7 Muir Wood D, Crewe A and Taylor C (2002). "Shaking table testing of geotechnical models". *International Journal of Physical Modelling in Geotechnics*, **1**: 01-13. https://doi.org/10.1680/ijpmg.2002.020101

8 Massimino MR and Maugeri M (2013). "Physical modelling of shaking table tests on dynamic soil-foundation interaction and numerical and analytical simulation". *Soil Dynamics and Earthquake Engineering*, **49**: 1-18. https://doi.org/10.1016/j.soildyn.2013.01.023

9 Chidichimo A, Cairo R, Dente G, Taylor CA and Mylonakis G (2014). "1-g experimental investigation of bi-layer soil response and kinematic pile bending". *Soil Dynamics and Earthquake Engineering*, **67**: 219-232. https://doi.org/10.1016/j.soildyn.2014.07.008

10 Simonelli AL, Di Sarno L, Durante MG, Sica S, Bhattacharya S, Dietz M, Dihoru L, Taylor CA, Cairo R, Chichidimo A, Dente G, Modaressi A, Todo Bom LA, Kaynia AM, Anoyatis G and Mylonakis G (2014). "*Experimental assessment of seismic pile-soil interaction*". Chapter 26 in *Seismic evaluation and rehabilitation of structures*.

11 Lanzano G, Bilotta E, Russo G, Silvestri F and Madabhushi GSP (2012). "Centrifuge modelling of seismic loading on tunnels in sand". *Geotechnical Testing Journal*, **35**(6): 854-869. https://doi.org/10.1520/GTJ104348

12 Conti R, Madabhushi GSP and Viggiani GMB (2012). "On the behavior of flexible retaining walls under seismic actions". *Géotechnique*, **62**(12): 1081-1094. https://doi.org/10.1680/geot.11.P.029

13 Kutter BL, Carey TJ, Hashimoto T, Zeghal M, Abdoun T, Kokkali P, Madabhushi GSP, Haigh SK, Burali d'Arezzo F, Madabhushi SPG, Hung W-Y, Lee C-J, Cheng H-C, Iai S, Tobita T, Ashino T, Ren J, Zhou Y-G, Chen Y-M, Sun Z-B and Manzari MT (2018). "LEAP-GWU-2015 experiment specifications, results and comparisons". *Soil Dynamics and Earthquake Engineering*, **113**: 616-628. https://doi.org/10.1016/j.soildyn.2017.05.018

14 Kutter BL, Carey TJ, Stone N, Li Zheng B, Gavras A, Manzari MT, Zeghal M, Abdoun T, Korre E, Escoffier S, Haigh SK, Madabushi GSP, Madabushi SSC, Hung W-Y, Liao T-W, Kim D-S, Kim S-N, Ha J-G, Kim NR, Okamura M, Sjafruddin AN, Tobita T, Ueda K, Vargas R, Zhou Y-G and Liu K (2019). "*LEAP-UCD-2017 Comparison of Centrifuge Test Results*". In: B. Kutter et al. (Eds.), *Model tests and numerical simulations of liquefaction and lateral spreading*: LEAP-UCD-2017. New York: Springer. https://doi.org/10.1007/978-3-030-22818-7_4

15 Tokimatsu K, Suzuki H and Sato M (2005). "Effects of inertial and kinematic interaction on seismic behaviour of pile with embedded foundation". *Soil Dynamics and Earthquake Engineering*, **25**(7-10): 753-762. https://doi.org/10.1016/j.soildyn.2004.11.018

16 Shirato M, Nonomura Y, Fukui J and Nakatani S (2008). "Large-scale shake table experiment and numerical simulation on the nonlinear behaviour of pile-groups subjected to large-scale earthquakes". *Soils and Foundations*, **48**(3): 375-396. https://doi.org/10.3208/sandf.48.375

17 Gajo A and Muir Wood D (1999a). "Severn-Trent sand: a kinematic hardening constitutive model for sands: the q-p formulation". *Géotechnique*, **49**(5): 595-614. https://doi.org/10.1680/geot.1999.49.5.595

18 Gajo A and Muir Wood D (1999b). "A kinematic hardening constitutive model for sands: the multiaxial formulation". *International Journal for Numerical and Analytical Methods in Geomechanics*, **23**(9): 925-965. https://doi.org/10.1002/(SICI)1096-9853(19990810)23:9<925::AID-NAG19>3.0.CO;2-M

19 Dafalias YF and Manzari MT (2004). "A simple plasticity sand model accounting for fabric change effects". *Journal of Engineering Mechanics*, **130**(6): 622-634. https://doi.org/10.1061/(ASCE)0733-9399(2004)130:6(622)

20 Dafalias YF, Papadimitriou AG and Li XS (2004). "Sand plasticity model accounting for inherent fabric anisotropy". *Journal of Engineering Mechanics*, **130**(11): 1319-1333. https://doi.org/10.1061/(ASCE)0733-9399(2004)130:11(1319)

21 Taiebat M and Dafalias YF (2008). "SANISAND: Simple anisotropic sand plasticity model". *International Journal for Numerical and Analytical Methods in Geomechanics*, **32**: 915-948. https://doi.org/10.1002/nag.651

22 Dafalias YF and Taiebat M (2016). "SANISAND-Z: Zero elastic range sand plasticity". *Géotechnique*, **66**(12): 999-1013. https://doi.org/10.1680/jgeot.15.P.271

23 Manzari MT and Dafalias YF (1997). "A critical state two-surface plasticity model for sands". *Géotechnique*, **47**(2): 255-272. https://doi.org/10.1680/geot.1997.47.2.255

24 Pisano F and Jeremic B (2014). "Simulating stiffness degradation and damping in soils via a simple visco-elastic-plastic model". *Soil Dynamics and Earthquake Engineering*, **63**: 98-109. https://doi.org/10.1016/j.soildyn.2014.02.014

25 Boulanger R and Ziotopoulou K (2015). "*PM4Sand Version 3: A sand plasticity model for earthquake engineering applications*". Technical Report. PM4Sand Files | PM4Sand (ucdavis.edu)

26 Kolymbas D (1991). "Computer-aided design of constitutive laws". *International Journal for Numerical and Analytical Methods in Geomechanics*, **15**: 593-604. https://doi.org/10.1002/nag.1610150806

27 Mašín D (2018). "*Modelling of soil behaviour with hypoplasticity. Another approach to soil constitutive modelling*". Springer.

28 Gudehus G (1996). "A comprehensive constitutive equation for granular materials". *Soils and Foundations*, **36**(1): 1-12. https://doi.org/10.3208/sandf.36.1

29 Von Wolffersdorff PA (1996). "A hypoplastic relation for granular materials with a predefined limit state surface". *Mechanics of Cohesive-Frictional Materials*, **1**(3): 251-271. https://doi.org/10.1002/(SICI)1099-1484(199607)1:3<251::AID-CFM13>3.0.CO;2-3

30 Niemunis A and Herle I (1997). "Hypoplastic model for cohesionless soils with elastic strain range". *Mechanics of Cohesive-Frictional Materials*, **2**: 279-299. https://doi.org/10.1002/(SICI)1099-1484(199710)2:4<279::AID-CFM29>3.0.CO;2-8

31 Wegener D (2013). "*Numerical investigation of permanent displacements due to dynamic loading*". PhD Thesis. Institut fur Geotechnik, TU Dresden, Germany.

32 Wegener D and Herle I (2014). "Prediction of permanent soil deformations due to cyclic shearing with a hypoplastic constitutive model". *Geotechnik*, **37**(2): 113-122. https://doi.org/10.1002/gete.201300013

33 Cudny M and Truty A (2020). "Refinement of the Hardening Soil model within the small strain range". *Acta Geotechnica*, **15**: 2031–2051. https://doi.org/10.1007/s11440-020-00945-5

34 Martinelli M, Burghignoli A and Callisto L (2016). "Dynamic response of a pile embedded into a layered soil". *Soil Dynamics and Earthquake Engineering*, **87**: 16-28. https://doi.org/10.1016/j.soildyn.2016.03.021

35 Miriano C, Cattoni E and Tamagnini C (2016). "Advanced numerical modelling of seismic response of a propped RC diaphragm wall". *Acta Geotechnica*, **11**(1): 161-175. https://doi.org/10.1007/s11440-015-0378-8

36 Kowalczyk P and Gajo A (2021). "Influence of pore pressure on natural frequency wandering of structures under earthquake conditions". *Soil Dynamics and Earthquake Engineering*, **142**: 106534. https://doi.org/10.1016/j.soildyn.2020.106534

37 Gajo A and Muir Wood D (1997). "*Numerical analyses of behaviour of shear stacks under dynamic loading*". Report on work performed under the EC project European Consortium of Earthquake Shaking Tables (ECOEST): Seismic bearing capacity of shallow foundations.

38 Pastor M, Zienkiewicz OC and Chan AHC (1990). "Generalized plasticity and the modelling of soil behaviour". *International Journal for Numerical and Analytical Methods in Geomechanics*, **14**: 151-190. https://doi.org/10.1002/nag.1610140302

39 Dar AR (1993). "*Development of a flexible shear-stack for shaking table testing of geotechnical problems*". PhD Thesis. University of Bristol, United Kingdom.

40 Abate G, Massimino MR, Maugeri M and Muir Wood D (2010). "Numerical modelling of a shaking table test for soil-foundation-superstructure interaction by means of a soil constitutive model implemented in a FEM Code". *Geotechnical and Geological Engineering*, **28**(1): 37-59. https://doi.org/10.1007/s10706-009-9275-y

41 Abate G and Massimino M (2016). "Dynamic soil-structure interaction analysis by experimental and numerical modelling". *Rivista Italiana di Geotecnica*, **2**: 44-70.

42 Régnier J, Bonilla L-F, Bard P-Y, Bertrand E, Hollender F, Kawase H, Sicilia D, Arduino P, Amorosi A, Asimaki D, Boldini D, Chen L, Chiaradonna A, DeMartin F, Elgamal A, Falcone G, Foerster E, Foti S, Garini E, Gazetas G, Gélis C, Ghofrani A, Giannakou A, Gingery J, Glinsky N, Harmon J, Hashash Y, Iai S, Kramer S, Kontoe S, Kristek J, Lanzo G, di Lernia A, Lopez-Caballero F, Marot M, McAllister G, Mercerat ED, Moczo P, Montoya-Noguera S, Musgrove M, Nieto-Ferro A, Pagliaroli A, Passeri F, Richterova A, Sajana S, Santisi d'Avila MP, Shi J, Silvestri F, Taiebat M, Tropeano G, Vandeputte D and Verrucci L (2018). "PRENOLIN: International benchmark on 1D nonlinear site-response analysis -validation phase exercise". *Bulletin of the Seismological Society of America*, **108**(2): 876-900. https://doi.org/10.1785/0120170210

43 Bilotta E, Lanzano G, Madabushi GSP and Silvestri F (2014). "A numerical Round Robin on tunnels under seismic actions". *Acta Geotechnica*, **9**: 563-579. https://doi.org/10.1007/s11440-014-0330-3

44 Manzari MT, El Ghoraiby M, Zeghal M, Kutter BL, Arduino P, Barrero AR, Bilotta E, Chen L, Chen R, Chiaradonna A, Elgamal A, Fasano G, Fukutake K, Fuentes W, Ghofrani A, Haigh SK, Hung W-Y, Ichii K, Kim DS, Kiriyama T, Lascarro C, Madabhushi GSP, Mercado V, Montgomery J, Okamura M, Ozutsumi O, Qiu Z, Taiebat M, Tobita T, Travasarou T, Tsiaousi D, Ueda K, Ugalde J, Wada T, Wang R, Yang M, Zhang J-M, Zhou Y-G and Ziotopoulou K (2019). "*LEAP-2017: Comparison of the Type-B Numerical Simulations with Centrifuge Test Results*". In: B. Kutter et al. (Eds.), *Model tests and numerical simulations of liquefaction and lateral spreading: LEAP-UCD-2017*. New York: Springer. https://doi.org/10.1007/978-3-030-22818-7_10

45 Ghofrani A and Arduino P (2018). "Prediction of LEAP centrifuge test results using a pressure-dependent bounding surface constitutive model". *Soil Dynamics and Earthquake Engineering*, **113**: 758-770. https://doi.org/10.1016/j.soildyn.2016.12.001

46 Gajo A (2010). "Hyperelastic modelling of small-strain anisotropy of cyclically loaded sand". *International Journal for Numerical and Analytical Methods in Geomechanics*, **34**(2): 111-134. https://doi.org/10.1002/nag.793

47 Durante MG (2015). "*Experimental and numerical assessment of dynamic soil-pile-structure interaction*". PhD Thesis. Università degli Studi di Napoli Federico II, Italy.

48 Kowalczyk P (2020). "*Validation and application of advanced soil constitutive models in numerical modelling of soil and soil-structure interaction under seismic loading*". PhD Thesis. University of Trento, Italy. https://dx.doi.org/10.15168/11572_275675

49 Kowalczyk P (2022). "Resonance of a structure with soil elastic waves released in nonlinear hysteretic soil upon unloading". *Studia Geotechnica et Mechanica*, **44**(4): 253–266. https://doi.org/10.2478/sgem-2022-0015

50 Kowalczyk P and Gajo A (2023). "Introductory consideration supporting the idea of the release of elastic waves in hysteretic soil". *Open Geomechanics*, **4**(4): 1-25. https://doi.org/10.5802/ogeo.16

51 Crewe AJ, Lings ML, Taylor CA, Yeung AK and Andrighetto R (1995). "*Development of a large flexible shear stack for testing dry sand and simple direct foundations on a shaking table*". European Seismic Design Practice, Elnashai (Ed), Balkema, Rotterdam.

52 Tan FSC (1990). "*Centrifuge and theoretical modelling of conical footings on sand*". PhD Thesis. University of Cambridge, United Kingdom.

53 Moccia F (2009). "*Seismic soil pile interaction: experimental evidence*". PhD Thesis. Universita degli Studi di Napoli Federico II, Italy.

54 Dassault Systèmes (2019). *Abaqus Standard software package*.

55 Gajo A (2019). *Fortran subroutine in a format of user defined material (UMAT) of the implementation of the Severn-Trent sand model*.

56 Been K and Jefferies MJ (1985). "A state parameter for sands". *Géotechnique*, **35**: 99-112. https://doi.org/10.1680/geot.1985.35.2.99

57 Gajo A and Bigoni D (2008). "A model for stress and plastic strain induced nonlinear, hyperelastic anisotropy in soils". *International Journal for Numerical and Analytical Methods in Geomechanics*, **32**: 833-861. https://doi.org/10.1002/nag.648

58 Dietz M and Muir Wood D (2007). "Shaking table evaluation of dynamic soil properties". *4th International Conference of Earthquake Geotechnical Engineering*, June 25-28, Thessaloniki, Greece.

59 Seed HB and Idriss IM (1970). "*Soil moduli and damping factors for dynamic response analysis*". EERC report 70-10. University of California, Berkeley

60 Kokusho T (1980). "Cyclic triaxial test of dynamic soil properties for wide strain range". *Soils and Foundations*, **20**(2): 45-60. https://doi.org/10.3208/sandf1972.20.2_45

61 Lambe T (1973). "Predictions in soil engineering". *Géotechnique*, **23**(2): 151-202.

62 Shahnazari H and Towhata I (2002). "Torsion shear tests on cyclic stress-dilatancy relationship of sand". *Soils and Foundations*, **42**(1): 105-119. https://doi.org/10.3208/sandf.42.105

63 Hardin BO and Black WL (1968). "Vibration modulus of normally consolidated clay". *Journal of the Soil Mechanics and Foundations Division (ASCE)*, **94**: 353-369. https://doi.org/10.1061/JSFEAQ.0001100

64 Watanabe K, Pisano F and Jeremic B (2017). "Discretization effects in the finite element simulation of seismic waves in elastic and elastic-plastic media". *Engineering with Computers*, **33**: 519-545. https://doi.org/10.1007/s00366-016-0488-4

65 Uesugi M and Kishida H (1986). "Influential factors of friction between steel and dry sands". *Soils and Foundations*, **26**(2): 33-46. https://doi.org/10.3208/sandf1972.26.2_33

66 Kuwano R and Jardine RJ (2002). "On the applicability of cross-anisotropic elasticity to granular materials at very small strains". *Géotechnique*, **52**: 727-749. https://doi.org/10.1680/geot.2002.52.10.727

67 Kowalczyk P (2023). "Some remarks on the performance of three advanced soil constitutive models in the small-strain region". *International Journal of Geotechnical Engineering*, **17**(3): 310-319. https://doi.org/10.1080/19386362.2023.2208917

68 Jardine R (1992). "Some observations on the kinematic nature of soil stiffness". *Soils and Foundations*, **32**(2): 111-124. https://doi.org/10.3208/sandf1972.32.2_111

69 Senetakis K, Madhusudhan BN and Anastasiadis A (2016). "Wave propagation and threshold strains of fully saturated soils with intraparticle voids". *Journal of Materials in Civil Engineering*, **28**(2): 1-11. https://doi.org/10.1061/(ASCE)MT.1943-5533.0001367

70 Roessett JM (1970). "*Fundamentals of soil amplification*". In *Seismic Design for Nuclear Power Plants*. The MIT Press, Cambridge, MA, 183-244.

71 Garini E, Anastasopoulos I and Gazetas G (2020). "Soil, basin and soil-building-soil interaction effects on motions of Mexico City during seven earthquakes". *Géotechnique*, **70**(7): 581-607. https://doi.org/10.1680/jgeot.18.P.314

72 Kowalczyk P (2022). "Proposal of a model setup for verification of the origin of high frequency motion in soil". *5th International Conference on New Developments in Soil Mechanics and Geotechnical Engineering*, 30 June-2 July, Nicosia, Northern Cyprus. https://link.springer.com/chapter/10.1007/978-3-031-20172-1_37

73 Kowalczyk P (2024). "*Experimental proof supporting the idea of elastic waves released in soil nonlinear small strain behaviour*" (Currently under development, title and authorship to be confirmed).

74 Kowalczyk P (2024). "New evidence on advantages of nonlinear site response analysis in modelling wave propagation in soil". *8th International Conference in Earthquake Geotechnical Engineering*, 7-10 May, Osaka, Japan. https://doi.org/10.3208/jgssp.v10.OS-3-01